

# Birefringent omnidirectional reflector

Kate Kaminska and Kevin Robbie

Anisotropic optical coatings offer unique polarizing properties, unmatched by conventional isotropic devices. Here we demonstrate the fabrication of a birefringent omnidirectional reflector, a type of photonic crystal, which exhibits complete reflection of radiation at 1.1  $\mu\text{m}$  for all incidence angles and polarizations. The thin-film device was deposited from electron-beam evaporated silicon, with refractive-index variation arising from atomic-scale porosity created with glancing-angle deposition. Birefringence was found to enhance the performance of the device compared with its isotropic counterpart by enlarging the photonic bandgap region of omnidirectional reflection. © 2004 Optical Society of America

OCIS codes: 160.4670, 310.1860, 310.6860, 230.4170, 230.1480.

## 1. Introduction

In recent years the optics community has dedicated great efforts toward the manufacture of a three-dimensional photonic crystal material that will enable efficient control of visible and infrared light particularly at wavelengths used in telecommunications. A photonic crystal with a complete three-dimensional bandgap restricts the propagation of light in a specified frequency for all directions of propagation and polarizations. Photonic crystals not only promise a variety of possible applications in lasers, wave guiding, switching, and computation, but also give rise to interesting new physics. The realization and efficient manufacture of such materials has proved challenging primarily because they require three-dimensional forms with small feature sizes (of the order of 100 nm). It has been demonstrated, however, that under certain conditions a one-dimensional photonic crystal structure, known as an omnidirectional reflector, can also restrict light propagation for all incidence angles.<sup>1,2</sup> The one-dimensional structure is much easier to fabricate than the three-dimensional photonic crystal, while still offering unique possibilities for light control.

In 1998 Fink *et al.*<sup>1</sup> fabricated the first omnidirectional reflector operating in the far-infrared part of

the electromagnetic spectrum and composed of alternating layers of polystyrene and tellurium. Since then research groups around the world have realized omnidirectional reflectors in the visible region with  $\text{Na}_3\text{AlF}_6/\text{ZnSe}$  (Ref. 3) and tin sulfide/silica (Ref. 4) multilayer structures and in the near infrared with amorphous silicon/silica (Ref. 5) and  $\text{GaAs}/\text{AlO}_3$  (Ref. 6) layers. All omnidirectional reflectors fabricated thus far have involved a combination of at least two deposition methods,<sup>1,3-6</sup> making the manufacturing process complex, time consuming, and expensive. We demonstrate an omnidirectional reflector operating at near-infrared wavelengths, made with an electron-beam evaporation technique, using a single source material. The refractive-index variation required for the high- and low-index regions of the omnidirectional stack was achieved by introduction of nanometer-scale porosity into the growing film by the technique of glancing-angle deposition<sup>7-9</sup> (GLAD). The microstructure of the film is anisotropic such that it induces optical form birefringence in the layers of the stack. As we demonstrate in this paper, the birefringence of the layers enhances the performance of the device compared with its isotropic counterpart by increasing the region of overlap between the stop bands observed for *p* and *s* polarizations, thereby enlarging the spectral width of the band of omnidirectional reflection.

## 2. Silicon Omnidirectional Reflector Produced with GLAD

It has been theoretically demonstrated that the necessary and sufficient criterion for omnidirectional reflection in a periodic one-dimensional system is that there be no propagating states within the system that

---

The authors are with the Department of Physics, Queen's University, Kingston, Ontario K7L 3N6, Canada. K. Kaminska's e-mail address is katekaminska@hotmail.com.

Received 5 August 2003; revised manuscript received 17 November 2003; accepted 8 December 2003.

0003-6935/04/071570-07\$15.00/0

© 2004 Optical Society of America

can couple to an incident propagating wave.<sup>1</sup> This is equivalent to requiring that there be a frequency range for which the band structures of the one-dimensional system and the ambient medium do not overlap.<sup>2</sup> This criterion may be satisfied by an endlessly repeating stack of dielectric films, which alternate in thickness between  $d_1$  and  $d_2$  and in refractive index between  $n_1$  and  $n_2$ . The indices  $n_1$  and  $n_2$  must be high enough that the Brewster angle  $\theta_B = \tan^{-1}(n_2/n_1)$ , at which there is no reflection for  $p$ -polarized light at any interface,<sup>10</sup> does not occur in the region of overlap between the band structure of the stack and that of the ambient medium. Selecting refractive indices  $n_1$  and  $n_2$  and thicknesses  $d_1$  and  $d_2$  to optimize the performance of an omnidirectional reflector is described in many theoretical investigations.<sup>1,2,11-13</sup>

Although the manufacture of an infinitely repeating stack of dielectric films is impossible in practice, transmitted light intensity diminishes exponentially with the number of layers, and a practical device with greatly reduced transmittance in a wide frequency range can be fabricated. We manufactured a 12-layer omnidirectional reflector with GLAD, using silicon as the source material. GLAD combines electron-beam evaporation onto a flat substrate in high vacuum with computer control of substrate tilt and rotation.<sup>7-9</sup> Refractive-index variation with a single source material is accomplished by introducing porosity into the film. The nanometer-scale porosity modulates the dielectric response such that the effective response of the material is approximately the density-weighted sum of the bulk material and ambient responses.<sup>14</sup>

In the GLAD process, vapor is obliquely incident onto the surface of a growing film, where previously deposited film material prevents subsequent deposition in its geometric shadow. Furthermore, the limited surface mobility of adatoms prevents film growth in shadowed regions, and an atomic-scale dendritic structure evolves, comparable with other diffusion-limited aggregation processes.<sup>15,16</sup> The film porosity is a strong function of the angle of arrival of the vapor flux onto the substrate, with porosity increasing with incidence angle. Films made at near normal incidence are essentially isotropic, as there is very little porosity. However, if a substrate is tilted at a fixed angle relative to the vapor flux and held motionless during deposition, the film grows inclined toward the source, producing an optically biaxial, birefringent medium.<sup>17</sup> When continuous, rapid substrate rotation is combined with vapor deposition at an angle, the resulting microstructure is pillarlike, extending perpendicular to the substrate.<sup>18</sup> This rotation eliminates in-plane anisotropy and produces a uniaxial, birefringent medium with the principal axis normal to the substrate surface. Figure 1 shows the geometry of the deposition process along with the resulting film structure and refractive-index directions.

Silicon was chosen to demonstrate omnidirectional reflection achieved by GLAD. Bulk silicon has a

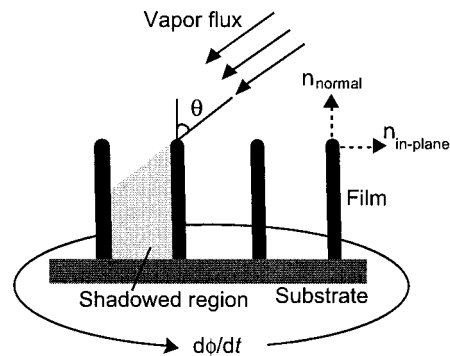


Fig. 1. Schematic of the deposition geometry of the GLAD process and the resulting film structure. The resulting principal refractive-index axes are indicated by dashed lines.

high index of refraction and is transparent in the infrared frequency range of the electromagnetic spectrum. Varying the porosity of a high-refractive-index bulk material such as silicon ( $n \approx 3.8$ ) between 0 and 1 produces a variation of index between 3.8 and approximately 1, as demonstrated with novel quintic antireflection coatings.<sup>19</sup> The optical response of the omnidirectional reflector was designed to have a high reflectivity around  $1.1 \mu\text{m}$  for any angle of light incidence. Winn *et al.*<sup>2</sup> demonstrated a range of possible values of the refractive indices of high- and low-index layers that satisfy the criteria for omnidirectional reflection. Given the range of index values attainable with GLAD evaporated silicon, the structure parameters were chosen to be  $n_1 = 1.9$ ,  $n_2 = 3.8$ ,  $d_1 = 216 \text{ nm}$ ,  $d_2 = 184 \text{ nm}$ .

Spectroscopic ellipsometry was performed on a set of eight 200-nm-thick films, manufactured at constant deposition angles on rotating substrates to establish a relation between deposition angle and the resulting refractive index of the film.<sup>19</sup> It was determined that deposition angles of  $65.6^\circ$  and  $0^\circ$  yield the desired in-plane indices of  $n_1 = 1.9$ ,  $n_2 = 3.8$  for the low- and high-index layers, respectively. Twelve alternating high- and low-index layers were vacuum evaporated at a pressure of  $10^{-7} \text{ Pa}$  ( $10^{-9} \text{ Torr}$ ) onto a Corning 7059 glass substrate by GLAD. The layer thickness was monitored during growth with a quartz crystal oscillation monitor. The deposition rate was maintained at  $0.5 \text{ nm/s}$ , the vapor flux angle was varied between  $65.6^\circ$  and  $0^\circ$ , and the substrate was continuously rotated at  $0.5 \text{ revolutions/s}$ . The 12-layer structure was characterized with a LEO 1530 field emission scanning electron microscope, and a micrograph of the fracture cross section of the device is presented in Fig. 2.

The optical response of the omnidirectional reflector was measured with a Woollam M-2000 spectroscopic ellipsometer in absolute transmission mode by using linearly polarized light. The apparatus allows measurement of transmittance through samples up to a light incidence angle of  $80^\circ$  from normal. The measured transmittance as a function of wavelength and incidence angle for  $s$ - and  $p$ -polarized light is

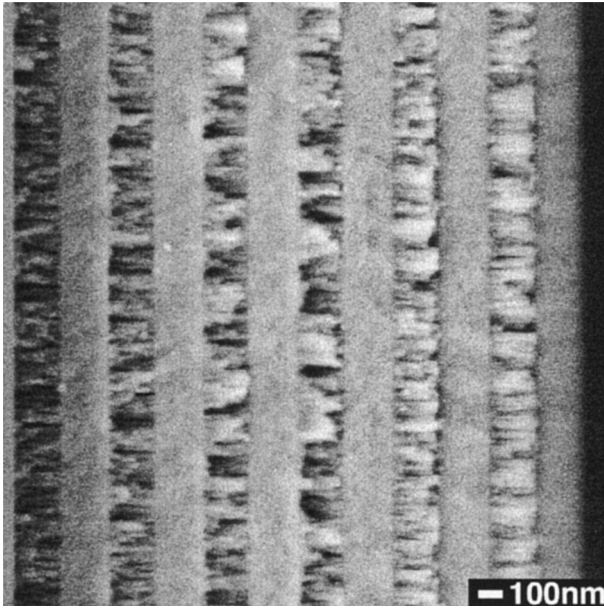


Fig. 2. Scanning electron micrograph of the cross section of the 12-layer silicon structure. The brighter, homogenous looking regions correspond to high-density (high-index) layers, and the darker regions correspond to low-density (low-index) layers.

shown in Fig. 3. As predicted, the omnidirectional reflector maintains very low transmissivity near 1.1  $\mu\text{m}$  for all incidence angles and polarizations. For all measured incidence angles the value of the transmission coefficient remained below 1.5% for *s* polarization and below 3% for *p* polarization in the bandgap region. The observed transmittance decrease below 1  $\mu\text{m}$  is consistent with silicon absorption.<sup>20</sup> Nonetheless, it is clear that the structure behaves as an omnidirectional reflector with a photonic bandgap at 1.1  $\mu\text{m}$ .

### 3. Birefringence

A dielectric medium is said to be anisotropic if its macroscopic properties depend on direction. In the case of optical anisotropy, or birefringence, the refractive index varies as a function of polarization as well as orientation with respect to the incident light wave.<sup>10</sup> Thin films that are deposited at an oblique angle exhibit birefringence owing to their columnar microstructure. The shape of the columns causes direction-dependent perturbations in the refractive index of the growing film.<sup>17</sup> The birefringence of the omnidirectional reflector was characterized with a Woollam M-2000 variable-angle spectroscopic ellipsometer with a spectral range of 370–1700 nm. Ellipsometric data was taken in  $2^\circ$  increments between  $50^\circ$  and  $80^\circ$  incidence angles. The ellipsometric model for each of the low-index layers was an effective medium approximation that mixed the optical constants of amorphous silicon with ambient air in a description of porous silicon. The effective medium model was further enhanced by separating the in-plane and normal optical response to model anisotropic effects. The experimental data were compared

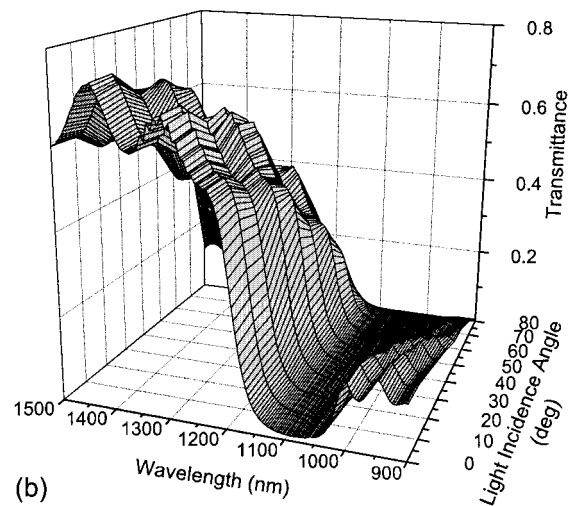
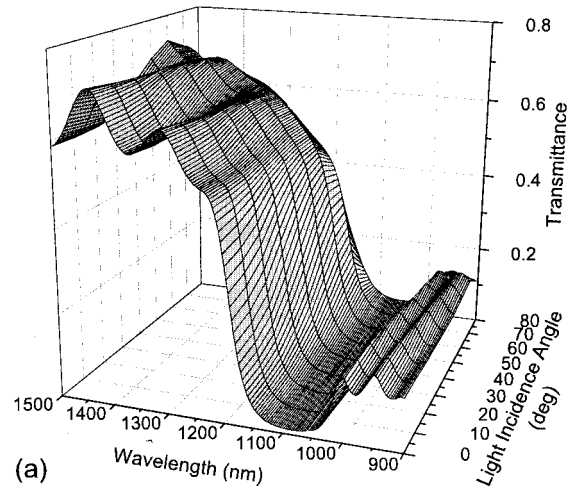


Fig. 3. Measured transmittance spectra of the birefringent omnidirectional reflector manufactured with GLAD: (a) *s*-polarized transmittance and (b) *p*-polarized transmittance as a function of wavelength and incidence angle. The bandgap of approximately zero transmittance at 1100 nm for both polarizations represents omnidirectional reflection.

with the generated model values by use of a mean squared error function. To find the model that best described the birefringent omnidirectional reflector, we minimized the error function by adjusting each fit parameter in a regression algorithm. At 1.1  $\mu\text{m}$  the resulting in-plane and normal refractive indices were  $n_{\text{in-plane}} = 1.99$  and  $n_{\text{normal}} = 2.12$  for the low-index layer and  $n_{\text{isotropic}} = 3.85$  for the high-index layer. Figure 4 shows the refractive-index depth profile of the omnidirectional reflector at 1.1  $\mu\text{m}$  as well as the dispersion of the dense and porous region indices as determined by ellipsometry.

The design of birefringent thin-film coatings requires a means of calculating the transmittance of the coatings at an arbitrary incidence angle. In 1997 Hodgkinson *et al.*<sup>21</sup> developed a compact eigenequation algorithm for computing light propagation through layered, optically anisotropic media.

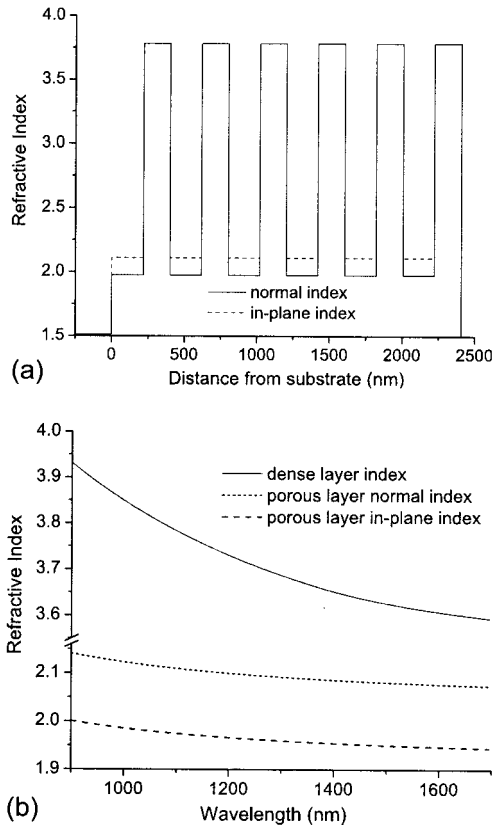


Fig. 4. Refractive indices of the omnidirectional stack as determined by variable-angle spectroscopic ellipsometry. (a) Refractive-index variation as a function of distance from the substrate at  $1.1 \mu\text{m}$ ; (b) wavelength dependence of the refractive index for the high-index isotropic layers and the low-index birefringent layers.

The algorithm uses Berreman calculus<sup>22</sup> to determine  $4 \times 4$  field matrices for each birefringent layer. A field matrix contains four basis field vectors, corresponding to two forward traveling waves and two backward traveling waves in each layer. The total field at any point in the medium may then be represented as the basis fields multiplied by complex coefficients. To allow comparison with experimental results, the eigenequation method outlined by Hodgkinson *et al.*<sup>21</sup> was implemented in the form of a MATLAB code and used to calculate the expected transmittance through the manufactured omnidirectional reflector for any range of incidence angles and wavelengths.

Figure 5 shows plots of measured and calculated transmittance for varying incidence angles and polarizations. The calculated transmittance is in reasonable agreement with the measured response. The measured transmittance is normalized to a measurement taken with no film or substrate in the path of the beam for a straight-through source to detector configuration. The decreased transmittance measured at short wavelengths is due to band-edge absorption in the silicon film. The calculated transmittance does not include this absorption or dif-

fuse scattering losses that occur because of the considerable surface roughness of GLAD films.<sup>19</sup> Volume scattering associated with bulk inhomogeneity and defects may also occur. As is shown in Fig. 4(b), the refractive-index dependence on wavelength is quite significant in the spectral range of interest, especially for the dense layer. The transmittance calculations therefore include a dispersion model consistent with the ellipsometry results.

The *s*-polarized transmittance is the same as it would be for an omnidirectional reflector made with isotropic layers, because at any incidence angle the electric field vector sees only the in-plane refractive index. However, in *p*-polarized light the electric field vector interacts with both the in-plane and the normal refractive indices and sees a different effective refractive index at every incidence angle. In Fig. 5 the plots showing *p*-polarized transmittance also include the calculated expected transmittance for an omnidirectional reflector with isotropic layers with indices  $n_1 = 1.99$ ,  $n_2 = 3.85$ , the same wavelength dependence as the birefringent layers, and thicknesses  $d_1 = 216 \text{ nm}$ ,  $d_2 = 184 \text{ nm}$ . The stop band for the isotropic device shifts away from  $1.1 \mu\text{m}$  toward lower wavelengths for more oblique incidence angles, relative to the birefringent device. As is shown in Section 4, it is the *p*-polarized transmittance that defines the higher wavelength edge of the omnidirectional range.<sup>1</sup> Therefore the bandgap for the birefringent device is larger than it would be for an isotropic equivalent.

#### 4. Band Structure

The allowed mode frequencies,  $\omega$ , for each choice of a wave vector,  $\mathbf{k}$ , comprise the photonic band structure. Since the manufactured device is not an infinitely repeating stack, there will be no absolute band structure, and modes will be allowed at every frequency. However, as the number of layers is increased, the transmittance decreases exponentially.<sup>2</sup> We may therefore plot a pseudo-band-structure showing regions of reduced transmittance that correspond to regions where no states would exist in an infinite structure. Figure 6 shows the pseudo-band-structure for the birefringent omnidirectional reflector. The gray areas highlight phase space regions of propagating states, whereas the white areas represent regions of exponentially reduced transmittance, which relate to forbidden states for an infinite structure. The transmittance threshold for the forbidden states was taken to be 3%. If a lower threshold is chosen, the *p*-polarization bandgap around  $\omega_n = 0.35$  closes. The plot was generated by our defining an orthogonal coordinate system  $xyz$  in which light propagates such that at the interface with the birefringent device axis  $x$  is perpendicular to the film surface and axes  $y$  and  $z$  are parallel to the surface. Without loss of generality, we assumed propagation in the  $x$ - $y$  plane and calculated transmittance by using the eigenequation method<sup>21</sup> for each value of  $k_y$  in the frequency range of interest. States with  $k_y = 0$  represent normal incidence. The normalized frequency

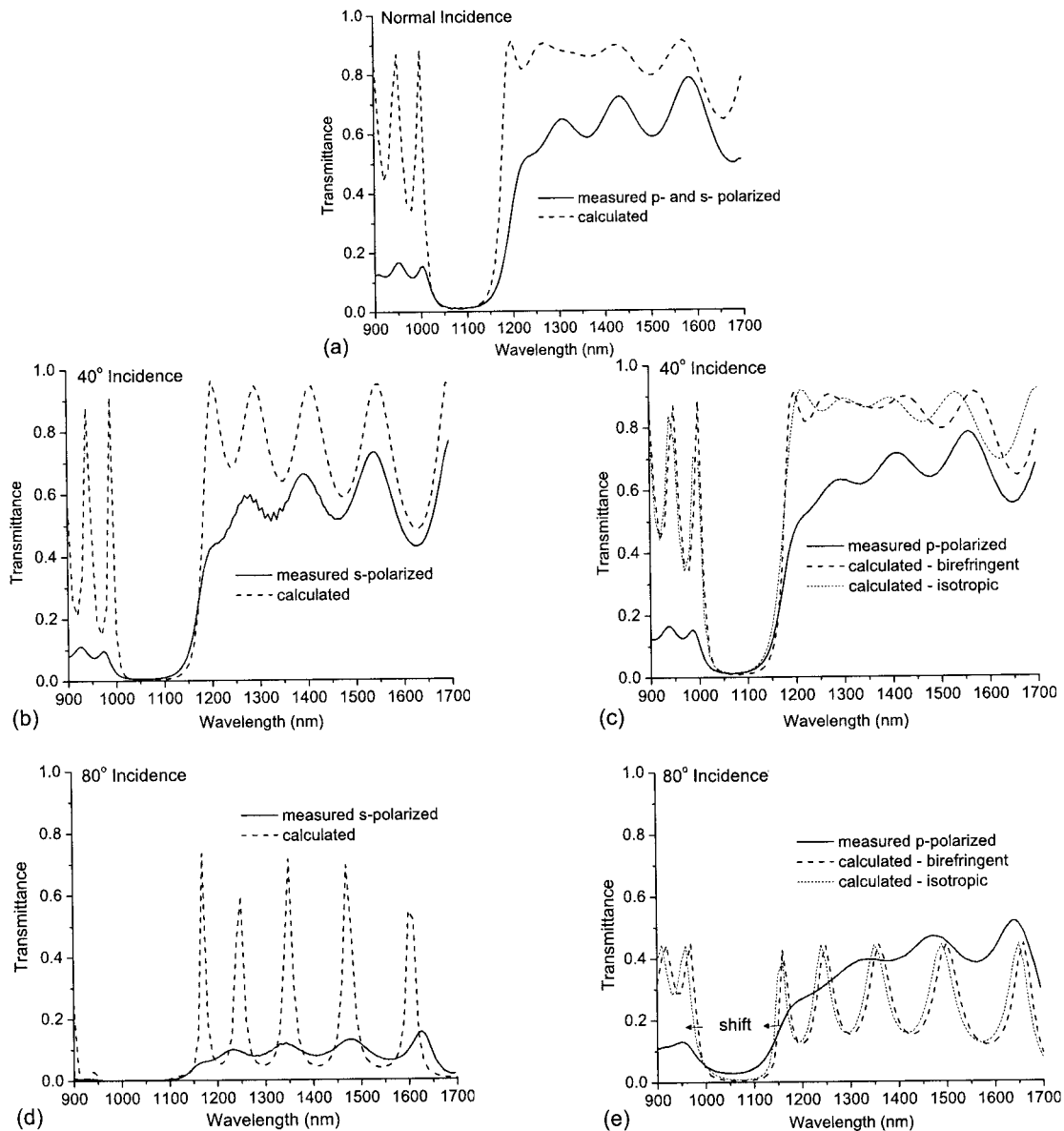


Fig. 5. Calculated (dashed curves) and measured (solid curves) transmittance as a function of wavelength for three angles of incidence. The plots corresponding to *p* polarization also include transmittance calculated for an isotropic device (dotted curve): (a) normal incidence, *p* and *s* polarized; (b) 40° incidence, *s* polarized; (c) 40° incidence, *p* polarized; (d) 80° incidence, *s* polarized; (e) 80° incidence, *p* polarized.

is defined as  $\omega_n = \omega a/c$ , where  $a = d_1 + d_2$  and  $c$  is the speed of light in the ambient medium. Since  $\omega = c(k_x^2 + k_y^2)^{1/2}$ , the modes for which  $\omega < ck_y$  were assigned zero transmittance, as these modes cannot exist in the ambient medium and therefore cannot couple to the device.

There are two frequency ranges in Fig. 4 in which no transmitting states exist, thereby satisfying the criterion for omnidirectional reflectivity.<sup>2</sup> Therefore there are two bandgaps in this birefringent system. The bandgap at  $\omega_n = 0.17$  corresponds to a wavelength of 2.3  $\mu\text{m}$ , and the other bandgap around  $\omega_n = 0.35$  corresponds to a wavelength of 1.1  $\mu\text{m}$ , which is the bandgap observed experimentally. The bandgap at  $\omega_n = 0.35$  is defined from above by the

normal-incidence band edge and from below by the *p*-polarization band edge. As shown in Section 3, the stop band of the isotropic device shifts away from 1.1  $\mu\text{m}$  toward higher frequencies (or lower wavelengths) relative to the stop band of the birefringent device, thereby shifting the *p*-polarization band edge toward higher frequencies. Therefore for an isotropic device the lower band edge of the omnidirectional range would occur at a higher frequency, whereas the upper band edge would remain the same as for the birefringent device. The bandgap of the birefringent omnidirectional reflector is therefore larger than that of an equivalent isotropic omnidirectional reflector. This observation is consistent with the numerical results obtained by Cojocaru<sup>23,24</sup> for anisotropic, peri-

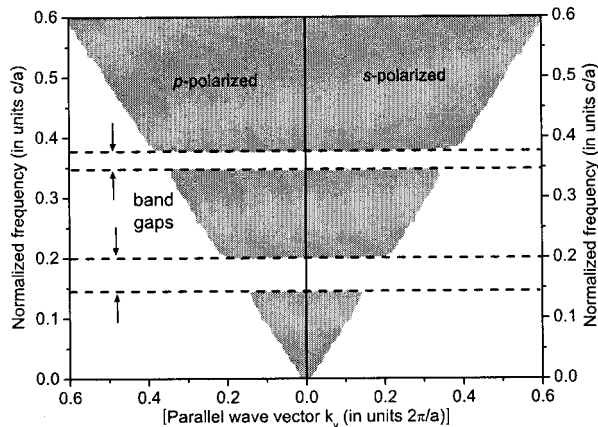


Fig. 6. Pseudo-band-structure of the birefringent omnidirectional reflector calculated by the eigenequation method. For an infinite structure, electromagnetic modes would exist only in the shaded regions. The white regions represent forbidden states. The *s*-polarized modes are plotted to the right of the origin, and the *p*-polarized to the left.

otic dielectric structures that demonstrated that introducing birefringence into the device layers results in a wider band of omnidirectional reflection than in an equivalent isotropic device.

## 5. Conclusions

We have shown through both experiment and calculation that a one-dimensional birefringent structure can exhibit omnidirectional reflection of incident radiation. This photonic crystal is fabricated with a modified thin-film deposition process in one step from a single source material. The reflector is expected to find use in integrated photonic systems for communications, sensing, etc. The omnidirectional behavior was examined in the spectral range of 370–1700 nm and angular light incidence range of 0°–80°. A wider spectral range and angular aperture was beyond the capability of the available apparatus; however, we were able to observe a predicted bandgap of the device at 1.1  $\mu\text{m}$ . The measured transmission coefficient in the omnidirectional range remained below 3%, and it can likely be enhanced with a larger number of layers. The performance of the device was shown to be superior to its isotropic counterpart. Good agreement was found between the measured and calculated spectra at normal, 40°, and 80° incidence. The discrepancies can be attributed to absorption and diffuse scattering losses.

A large number of potential applications exist for GLAD-manufactured films in optics. Liquid-crystal infiltration<sup>25</sup> into the film pores will allow electro-optic control, and fluid or gas permeation<sup>26</sup> will allow a controlled shift of the optical response. Structural ordering in the plane of the substrate is expected to produce resonant scattering, and higher-order photonic crystal effects.<sup>27,28</sup>

This work was supported by the Natural Sciences and Engineering Research Council of Canada, the

Canadian Institute for Photonic Innovation, and the Canada Research Chairs program.

## References

1. Y. Fink, J. N. Winn, S. Fan, C. Chen, J. Michel, J. D. Joannopoulos, and E. L. Thomas, "A dielectric omnidirectional reflector," *Science* **282**, 1679–1682 (1998).
2. J. N. Winn, Y. Fink, S. Fan, and J. D. Joannopoulos, "Omnidirectional reflection from a one-dimensional photonic crystal," *Opt. Lett.* **23**, 1573–1575 (1998).
3. D. N. Chigrin, A. V. Lavrienko, D. A. Yarotsky, and S. V. Gaponenko, "Observation of total omnidirectional reflection from a one-dimensional dielectric lattice," *Appl. Phys. A* **68**, 25–28 (1999).
4. M. Deopura, C. K. Ullal, B. Temelkuran, and Y. Fink, "Dielectric omnidirectional visible reflector," *Opt. Lett.* **26**, 1197–1199 (2001).
5. B. Gallas, S. Fisson, E. Charron, A. Brunet-Bruneau, G. Vuye, and J. Rivory, "Making an omnidirectional reflector," *Appl. Opt.* **40**, 5056–5063 (2001).
6. Y. Park, Y. Roh, C. Cho, H. Jeon, M. G. Sung, and J. C. Woo, "GaAs-based near infrared omnidirectional reflector," *Appl. Phys. Lett.* **82**, 2770–2772 (2003).
7. K. Robbie, M. J. Brett, and A. Lakhtakia, "Chiral sculpted thin films," *Nature* **384**, 616–616 (1996).
8. K. Robbie, A. J. P. Hnatiw, M. J. Brett, R. I. MacDonald, and N. J. McMullin, "Inhomogeneous thin film optical filters fabricated using glancing angle deposition," *Electron. Lett.* **33**, 1213–1214 (1997).
9. K. Robbie and M. J. Brett, "Sculptured thin films and glancing angle deposition: growth mechanics and applications," *J. Vac. Sci. Technol. A* **15**, 1460–1465 (1997).
10. B. E. A. Saleh and M. C. Teich, *Fundamentals of Photonics* (Wiley, New York, 1991).
11. W. H. Southwell, "Omnidirectional mirror design with quarter-wave dielectric stacks," *Appl. Opt.* **38**, 5464–5467 (1999).
12. S. Kim and C. K. Hwangbo, "Design of omnidirectional high reflectors with quarter-wave dielectric stacks for optical telecommunication bands," *Appl. Opt.* **41**, 3187–3192 (2002).
13. X. Wang, X. Hu, Y. Li, W. Jia, C. Xu, X. Liu, and J. Zi, "Enlargement of omnidirectional total reflection frequency range in one-dimensional photonic crystals by using photonic heterostructures," *Appl. Phys. Lett.* **80**, 4291–4293 (2002).
14. S. Bosch, J. Ferre-Borrull, N. Leinfellner, and A. Canillas, "Effective dielectric function of mixtures of three or more materials: a numerical procedure for computations," *Surf. Sci.* **453**, 9–17 (2000).
15. R. Messier, V. C. Venugopal, and P. D. Sunal, "Origin and evolution of sculptured thin films," *J. Vac. Sci. Technol. A* **18**, 1538–1545 (2000).
16. L. Abelmann and C. Lodder, "Oblique evaporation and surface diffusion," *Thin Solid Films* **305**, 1–21 (1997).
17. I. J. Hodgkinson and Q. Hong Wu, *Birefringent Thin Films and Polarizing Elements* (World Scientific, Singapore, 1997).
18. K. Robbie, C. Shafai, and M. J. Brett, "Thin films with nanometer-scale pillar microstructure," *J. Mater. Res.* **14**, 3158–3163 (1999).
19. K. Kaminska, T. Brown, G. Beydaghyyan, and K. Robbie, "Vacuum evaporated porous silicon photonic interference filters," *Appl. Opt.* **42**, 4212–4219 (2003).
20. E. D. Palik, *Handbook of Optical Constants of Solids* (Academic, New York, 1985).
21. I. J. Hodgkinson, S. Kassam, and Q. H. Wu, "Eigenequations and compact algorithms for bulk and layered anisotropic op-

- tical media: reflection and refraction at a crystal–crystal interface,” *J. Comput. Phys.* **133**, 75–83 (1997).
22. D. W. Berreman, “Optics in stratified and anisotropic media:  $4 \times 4$ -matrix formulation,” *J. Opt. Soc. Am.* **62**, 502–510 (1972).
  23. E. Cojocaru, “Omnidirectional reflection from Šolc-type anisotropic periodic dielectric structures,” *Appl. Opt.* **39**, 6441–6447 (2000).
  24. E. Cojocaru, “Omnidirectional reflection from finite periodic and Fibonacci quasi-periodic multilayers of alternating isotropic and birefringent thin films,” *Appl. Opt.* **41**, 747–754 (2002).
  25. K. Robbie, D. J. Broer, and M. J. Brett, “Chiral nematic order in liquid crystals imposed by an engineered inorganic nanostructure,” *Nature* **399**, 764–766 (1999).
  26. P. A. Snow, E. K. Squire, P. St. J. Russell, and L. T. Canham, “Vapor sensing using the optical properties of porous silicon Bragg mirrors,” *J. Appl. Phys.* **86**, 1781–1784 (1999).
  27. O. Toader and S. John, “Proposed square spiral microfabrication architecture for large three-dimensional photonic bandgap crystals,” *Science* **292**, 1133–1135 (2001).
  28. O. Toader and S. John, “Square spiral photonic crystals: robust architecture for microfabrication of materials with large three-dimensional photonic bandgaps,” *Phys. Rev. E* **66**, 016610/1–18 (2002).